NUCL SCI TECH (2017) 28:44
DOI 10.1007/s41365-017-0201-3

Energy-spread measurement of triple-pulse electron beams based on the magnetic dispersion principle

Yi Wang[1] · Qin Li[1] · Zhi-Yong Yang[1] · Huang Zhang[1] · Heng-Song Ding[1] · An-Min Yang[1] · Min-Hong Wang[1]

Received: 18 April 2016 / Revised: 26 May 2016 / Accepted: 3 June 2016 / Published online: 27 February 2017

Abstract The method of energy dispersion in magnetic field is used to analyze the energy spread of the triple-pulse electron beam generated by the Dragon-II linear induction accelerator. A sector magnet is applied for energy analysis of the electron beam, with a bending radius of 300 mm and a deflection angle of 90°. For each pulse, the time-resolved and integral images of the electron position at the output port of beam-bending line are recorded by a streak camera and a CCD camera, respectively. Experimental results demonstrate an energy spread of less than ±2.0% for the electron pulses. The cavity voltage waveforms obtained by different detectors are also analyzed for comparison.

Keywords Energy spread · Linear induction accelerator · Magnetic dispersion

1 Introduction

The linear induction accelerator (LIA) is able to generate pulsed charged particle beams of extremely high currents, which has been well developed and widely applied in various fields, such as flash radiography [1], high-power microwave generation [2] and heavy ion fusion [3, 4]. In order to investigate the hydrodynamic process of high explosives, MeV electron beam pulses generated in LIA are focused onto a high-Z convertor to produce X-rays photons through the bremsstrahlung [5]. The temporal width of the pulse is typically tens of nanoseconds, which is capable of recording an inner stopped-motion image of a dense object with a relatively small motion blur. For obtaining fine details of the acquired image, it is strongly demanded to reduce the X-ray spot size as small as possible, which is quoted as the evaluation of the resolving ability.

However, reducing the X-ray spot size is limited by factors of the space-charge effect, spherical aberration of the lens, the beam emittance, the energy spread, etc. [6]. The beam energy spread affects the spot size in two ways: the minimal beam spot radius determined by dispersion aberration of the lens depends directly on energy spread of the electron beam [7]; and the beam energy spread aggravates the Corkscrew oscillation induced by the titled beam injection, an inaccurate alignment of the solenoidal field, giving rise to a bigger spot size and a larger spatial jitter [8]. So, the beam energy spread is mainly determined by waveform and synchronization of the induction accelerating voltages, and the load effect of intense beam [9].

In this paper, a method based on magnetic dispersion is used to measure the energy spread of triple-pulse electron beams produced by the Dragon-II LIA. The cavity voltage waveforms detected by the capacitor voltage probe (CVP) and resistor voltage divider (RVD) are analyzed for comparison.

2 Principle of magnetic dispersion

In a magnetic field, electrons in different energies move along distinct bending orbits. Such a spatial dispersion of charged particles results from the effect of Lorentz force,

✉ Yi Wang
wangyi_caep@163.com

[1] Key Laboratory of Pulsed Power, Institute of Fluid Physics, China Academy of Engineering Physics, Mianyang 621900, China

which serves as the centripetal force of the deflection perpendicular to the particle motion and the magnetic field. This follows the relation of [10]

$$mv^2/\rho = evB, \tag{1}$$

where m is the particle mass, v is the scalar velocity, ρ is bending radius of the orbit, e is the electron charge, and B is magnetic induction intensity perpendicular to velocity. The momentum ($p = mv$) of a relativistic electron can be expressed as

$$p = \beta\gamma m_0 c, \tag{2}$$

where $\beta = v/c$ with c being the light velocity in vacuum, $\gamma = (1-\beta^2)^{-1/2}$ is the relativistic factor, and m_0 is the rest mass of electron. The kinetic energy E_k is given by

$$E_k = (\gamma - 1)m_0c^2. \tag{3}$$

Substituting Eqs. (1) and (2) into (3), one has Eq. (4) to relate the electron kinetic energy and orbit curvature radius,

$$E_k = m_0c^2\left[\sqrt{1+\left(\frac{eB\rho}{m_0c}\right)^2} - 1\right]. \tag{4}$$

For a sector magnet with uniform magnetic field and normal entry and exit, the radial coordinates (x_1, x_2) and the slopes (x'_1, x'_2) of a trajectory at two positions are linked with the momentum deviation $\Delta p/p_0$ by the transfer matrices [11], i.e.,

$$\begin{pmatrix} x_2 \\ x'_2 \\ \frac{\Delta p}{p_0} \end{pmatrix} = \begin{pmatrix} 1 & L_2 & 0 \\ 0 & 1 & 0 \\ 0 & 0 & 1 \end{pmatrix} \begin{pmatrix} \cos\varphi & \rho_0\sin\varphi & \rho_0(1-\cos\varphi) \\ -\frac{1}{\rho_0}\sin\varphi & \cos\varphi & \sin\varphi \\ 0 & 0 & 1 \end{pmatrix} \times \begin{pmatrix} 1 & L_1 & 0 \\ 0 & 1 & 0 \\ 0 & 0 & 1 \end{pmatrix} \begin{pmatrix} x_1 \\ x'_1 \\ \frac{\Delta p}{p_0} \end{pmatrix}, \tag{5}$$

where L_1 and L_2 are the objective and image distances, respectively; φ is the deflection angle; and ρ_0 is the bending radius of the central ray inside the magnetic field. Usually, a slit is designed and installed at the center of the input port, which denotes the radial coordinate of the object position to as $x_1 = 0$. Considering the symmetric drift-space of $L_1 = L_2 = \rho_0$ and the bending angle of $\varphi = 90°$, the relation between the momentum difference and trajectory parameters can be simplified as

$$\frac{\Delta p}{p} = \frac{x_2}{2\rho_0}, \tag{6}$$

Then, the corresponding difference in kinetic energy is given by

$$\frac{\Delta E_k}{E_{k0}} = \frac{\gamma+1}{\gamma}\frac{x_2}{2\rho_0}, \tag{7}$$

where E_{k0} is the kinetic energy of the electron moving on the reference trajectory ($\rho = \rho_0$). It can be seen that the radial coordinate of the trajectory at the image plane depends just on the kinetic energy, rather than the slope at the object position. Figure 1 shows the numerically calculated orbits of the electrons, which have distinct image positions for different kinetic energies (18.5 and 19.5 MeV). The drift spaces before and after the magnetic field ($B = 2170$ Gs) are both 300 mm in length. The reference orbit inside the magnetic field has a bending radius of 300 mm and a deflection angle of 90°. The electrons of the same kinetic energy are focused to the same point on the image plane though starting with different azimuth angles. By measuring the image position with respect to the reference trajectory, the electron beam energy can be obtained and the energy spread is then calculated by

$$\varepsilon = \pm\frac{E_{k,max} - E_{k,min}}{2E_{k,mean}} \times 100\%, \tag{8}$$

where $E_{k,max}$, $E_{k,min}$ and $E_{k,mean}$ are the maximum, minimum and mean kinetic energies, respectively, corresponding to the maximum, minimum and mean x_2.

3 Experimental setup and measurements

As shown in Fig. 2, a pair of 1-mm graphite slits with an axial length of 80 mm is fixed on input port of the vacuum tube, which restricts entrance position of the electrons

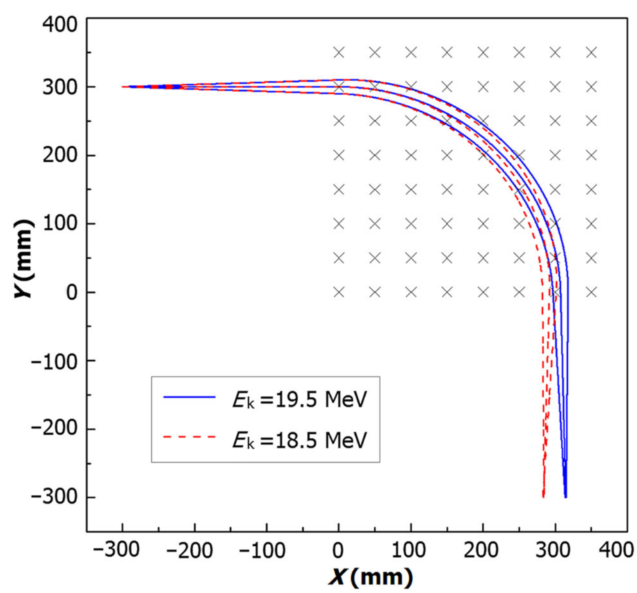

Fig. 1 (Color online) Energy dispersion of the electron beam in the magnetic field, at the magnetic induction intensity of $B = 2170$ Gs

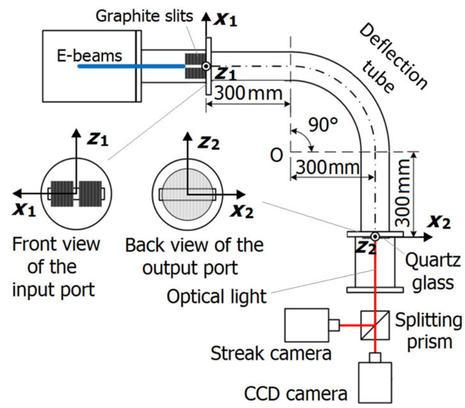

Fig. 2 (Color online) Schematics for the energy-spread measurement

exactly on the central trajectory. A sector magnet in bending radius of 300 mm and deflection angle of 90° is carefully constructed on the beam line for measurement. The magnet is designed and modified to ensure that effective edges of the magnetic extended fringing field match with the deflection part of the tube. The object- and image-side drift spaces are both 300 mm in length. A quartz glass is placed at the output port to generate optical photons through Cherenkov radiation [12] when the electrons exit the tube and impinge on the glass. The optical light is split by a prism and received by a streak camera and a CCD camera, respectively. The streak camera records a continuous time-resolved image position during a pulse. The CCD camera, which is coupled with a micro-channel plank for gating-time control, records the integrated image of a whole pulse. To provide a stable uniform magnetic field, a power supply is used to load a constant current on the excitation coil of the magnet. The corresponding relation between the magnetic intensity and the loaded current has been scaled with a Gaussmeter in advance. The stabilized current is limited within 10 mA, which denotes a magnetic field fluctuation of less than 5 Gs during the measurement.

Experiments are carried out on the Dragon-II LIA for energy-spread measurement of the electron beams. At a time in one experiment, three electron pulses (Pulses A, B and C) are generated, with a time gap of $\sim$400 ns between two neighboring pulses. For each measurement, the external signal for triggering the cameras is tuned to synchronize with an electron pulse to be detected. The time-solved and integrated images are recorded at the exit port, by which energy spread of the electron beam can be calculated according to the relation between the electron energy and the image position.

4 Results and discussion

For each experiment, a triple-pulse electron beam passes through the magnetic analyzer, among which the image of one chosen pulse at the exit port is recorded. The alternation

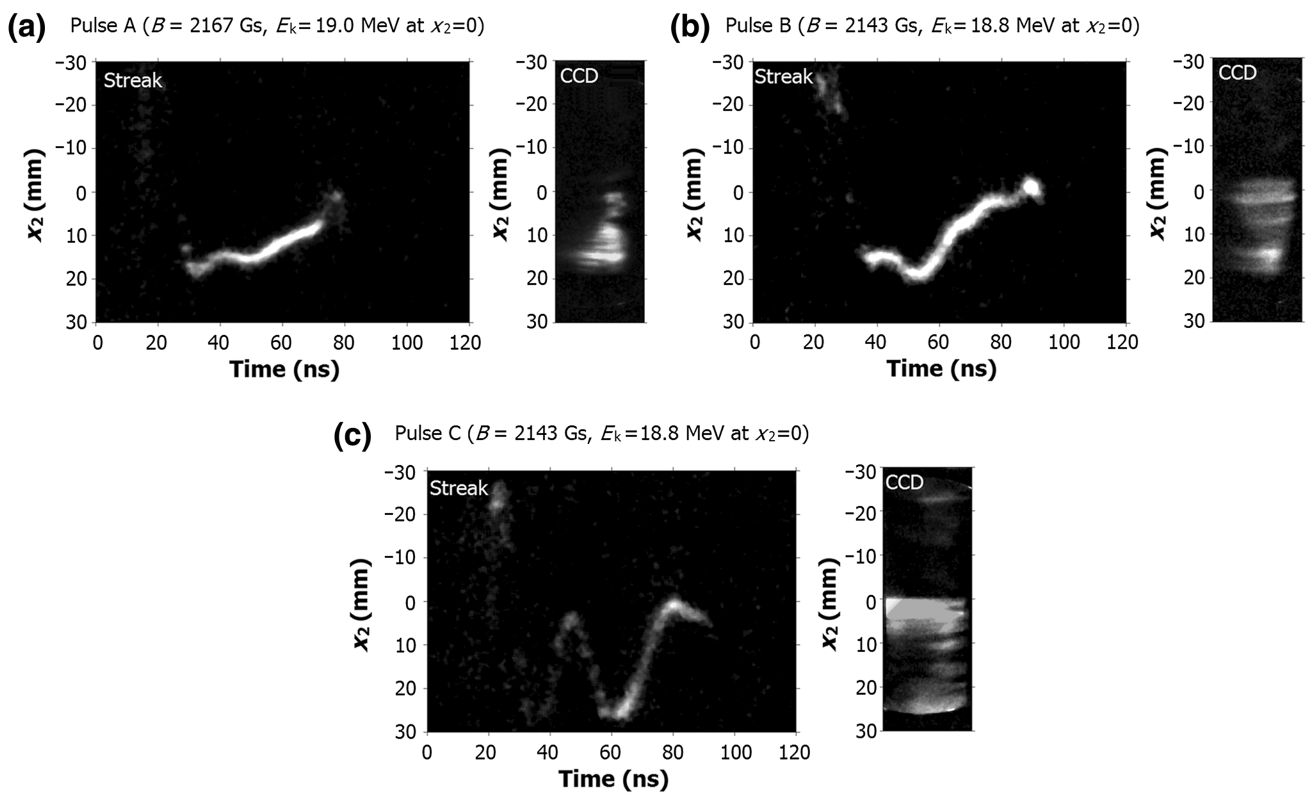

Fig. 3 Images captured by streak camera (*left*) and CCD camera (*right*)

of image position actually denotes changes in electron energy during the pulse. The images captured by the streak and CCD cameras in the measurements are shown in Fig. 3. A pair of graphite slits is installed at the streak camera entry to further limit the image in the z-axis, (perpendicular to the slits). So the energy of an electron pulse manifests itself as a continuously time-variable spot position on the streak camera image. The CCD camera records an integral image of the electron at the tube exit port, with the image width in x-axis represents the energy range of a whole pulse. The experimental results are listed in Table 1. We mainly consider the flat top part of the electron beam pulse, which is $\sim$50 ns for Pulse A and $\sim$60 ns for Pulses B and C. The results reveal that the energy spread of the flat top of electron beam pulse is not more than ±2.0%. Specifically, Pulse A has the smallest energy spread ($\varepsilon = \pm 1.35\%$), while pulse C has the largest one ($\varepsilon = \pm 1.95\%$).

The energy spread of electron beam mostly results from imperfect square voltage waveforms and asynchrony between different accelerating cavities. The triple-pulser of the Dragon-II LIA consists of three square-pulse sections, a confluent/blocking network, and a control/triggering modular unit [13, 14]. The pulser is designed for load-matching, which helps to reduce reflections of the pulses but still cannot completely eliminate the effect. The former voltage pulse(s) will be reflected to add on the latter one(s). So, generally, a former electron beam pulse has a smaller energy spread than a latter one does.

The cavity voltage waveform is detected by the CVP and RVD. As shown in Fig. 4, the waveforms obtained by the two probes slightly differ from each other at the flat top part. The detected waveform is closely related to the time difference between the voltage signal and the beam-load signal arriving at the detector. The CVP is located close to the accelerating gap, while the RVD is outside the cavity. Thus, the CVP is expected to provide a waveform closer to the real one. This is verified by the fact that the CVP waveform accords much better with the result of magnetic

Table 1 Experimental results of the energy-spread measurement

No.	Pulse	B (Gs)	τ_{flat} (ns)	X_2 (mm)			E_k (MeV)			ε
				Min	Max	Mean	Min	Max	Mean	
#1	A	2167	50	1.5	17.4	9.5	19.03	19.55	19.29	±1.35%
#2	B	2143	60	−1.0	18.2	8.6	18.74	19.36	19.05	±1.63%
#3	C	2143	60	1.7	25.3	13.5	18.83	19.58	19.21	±1.95%

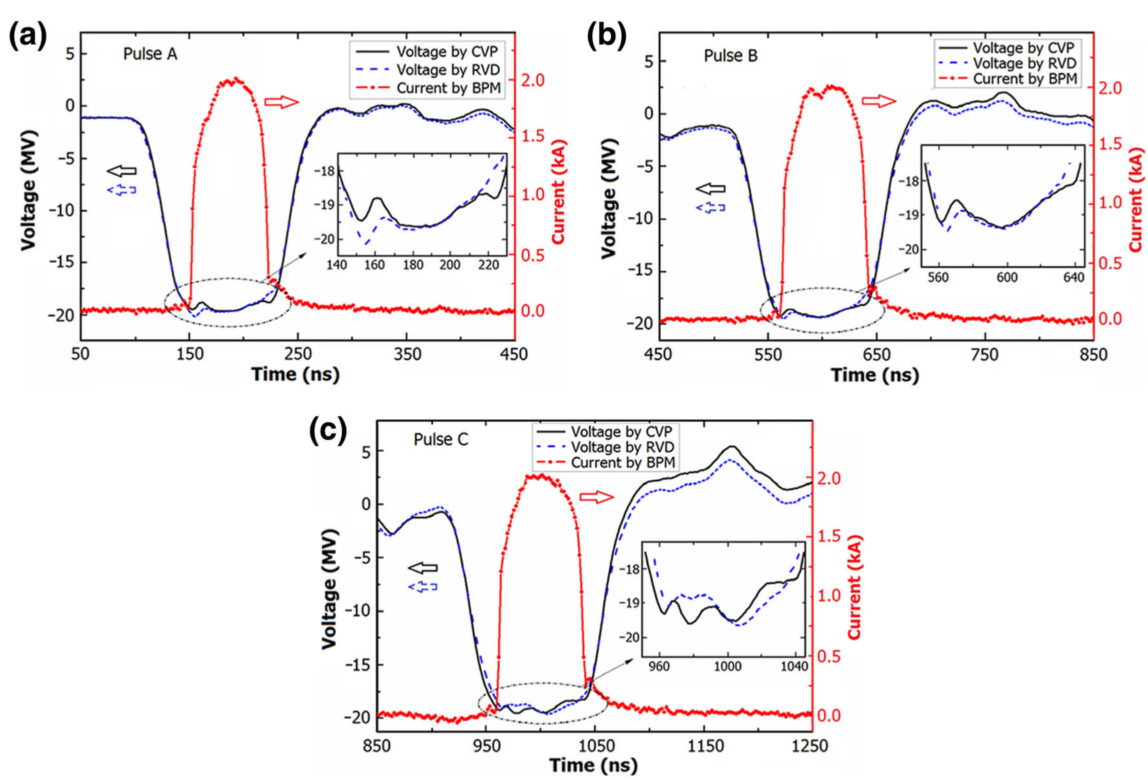

Fig. 4 (Color online) Voltage and current waveforms of electrical signals

analysis. The current waveform obtained by the beam position monitor (BPM) at upstream of the tube indicates that the camera images correspond to the central part of the electron beam. Current of the electron beam reaches $\sim$2 kA for all the triple pulses. For a relativistic paraxial beam, the focusing magnetic force almost balances the electric repulsion, which is independent of the beam geometry [11]. The space-charge effect barely impacts on the beam transport, hence the energy analysis.

The error of the experiment mainly results from inaccuracy of the magnetic field intensity, and deviation of the electron position. The first part includes the accuracy of magnet scaling and instability of the current loaded, which give an error of less than 15 Gs in the magnetic field intensity. The second part includes deviations in positioning the input graphite slits, the deflection tube and the magnet, which correspond to an error of totaling 4 mm in the image position at the output port. The error of the kinetic energy is calculated at 0.27 MeV at $E_{k,} = \sim 19$ MeV. Because the energy spread is a relative difference of the kinetic energy, the energy-spread error is mainly determined by the graphite slit width and the discrimination of electron position from the image. Then, the energy-spread error is calculated at $\varepsilon_{error} = 0.68\%$ (absolute value) in the experiment.

According to the beam current waveforms, the charge in the electron beam is calculated at 1.3×10^{-4} C for Pulse A and 1.5×10^{-4} C for Pulses B and C. The slit width at the input port restricts most of the beam current from entering the deflection magnetic field. Due to the axial length of the graphite slits, the slit width also limits the angular width of the electron beam. It mainly blocks off the rising and falling parts of the beam pulse, which appear to oscillate much more fiercely than the flat-top part does. Considering a Gaussian beam profile with a RMS radius of 10 mm, the slit width (1 mm in the x-direction) and the tube width (20 mm in the z-direction) allow an entrance charge of about 3.0×10^{-6} for Pulse A and 3.6×10^{-6} C for Pulses B and C. Because the resolving power of the electron momentum (or energy) is inversely proportional to the input slit width, a larger slit width enhances the signal of measurement, with a loss in the resolving power, though.

5 Conclusion

The method of magnetic analyzing is applied to measure the energy spread of the triple-pulse electron beam produced by the Dragon-II LIA. The beam line for diagnostic is designed to have symmetric drift-space lengths at the upstream and downstream of the sector magnet, which has a bending radius of 300 mm and a deflection angle of 90°. The energy spread of the electron beam for different pulses are all within $\pm 2.0\%$ for the flat-top part. Due to the effect of the cavity voltage reflection, the first pulse of the electron beam has the smallest energy spread, while the last pulse has the largest one. Due to the time difference caused by the cavity structure, the voltage waveforms detected by the CVP and RVD show to be slightly different at the flat top. Since the location of the CVP is very close to the accelerating gap, it is expected to provide an exact cavity voltage. Experimental results display a good agreement between the CVP waveform and the energy spectrum of the magnetic analyzer.

References

1. R. D. Scarpetti, J. K. Boyd, G. G. Earley, et al., Upgrades to the LLNL Flash X-ray Induction Linear Accelerator (FXR), in *11th IEEE International Pulsed Power Conference—Digest Of Technical Papers*, vol 1&2, p. 597–602 (1997). doi: 10.1109/PPC.1997.679405
2. E. B. Abubakirov, O.V. Arkhipov, L.V. Bobyleva, et al., Generation and Acceleration of High-current Annular Electron-beam in Linear Induction Accelerator and Microwave-power from Cherenkov TWT, in *Epac 90, 2nd European Particle Accelerator Conference*, vol. 1&2, p. 34–36 (1990)
3. W.M. Fawley, T. Garvey, S. Eylon et al., Beam dynamics studies with the heavy-ion linear induction accelerator MBE-4. Phys. Plasmas **4**(3), 880–894 (1997). doi:10.1063/1.872147
4. V.I. Karas, O.V. Manuilenko, V.P. Tarakanov et al., Stability of the high-current ion beam in drift gap of linear induction accelerator. Probl. At. Sci. Technol. **54**, 64–68 (2013)
5. C. Ekdahl, E. O. Abeyta, L. Caudill, et al., First Beam at DARHT-II, in *Proceedings of the 2003 Particle Accelerator Conference*, vol 1–5, p. 558–562 (2003). doi:10.1109/pac.2003.1288976
6. J. Shi, Y. Lin, B. Ding, Limiting of the spot size of intense relativistic electronic beams in a solenoid field. High Power Laser Part. Beams **13**(02), 245–249 (2001). **(in Chinese)**
7. P. Dong, Z. Dai, Y. Xie et al., Particle-in-cell simulation on focusing of intense electron beam. High Power Laser Part. Beams **24**(8), 1970–1974 (2012). **(in Chinese)**
8. Y.J. Chen, Corkscrew modes in linear accelerators. Nucl. Instrum. Methods Phys. Res. Sect. A **292**(2), 455–464 (1990). doi:10.1016/0168-9002(90)90403-s
9. H. Zhang, Y. Wang, T.T. Li et al., Beam load effect on the cavity voltage waveform in linear induction accelerators. High Power Laser Part. Beams **28**(01), 28015101 (2016). **(in Chinese)**
10. K.H. Zhao, X.M. Chen, *Electromagnetics* (Higher Education Press, Beijing, 2003). **(in Chinese)**
11. J.Q. Lv, *The Optics of Charged Particle Beams* (Higher Education Press, Beijing, 2004). **(in Chinese)**
12. E.P. Cherenkova, The discovery of the Cherenkov radiation. Nucl. Instrum. Methods Phys. Res. Sect. A **595**(1), 8–11 (2008). doi:10.1016/j.nima.2008.07.006
13. S.F. Chen, X. Li, Z.P. Huang et al., Output of triple-pulse megahertz burst rate high-voltage induction device. Appl. Phys. Lett. **88**(26), 264107 (2006). doi:10.1063/1.2213183
14. S.F. Chen, J.J. Deng, X. Li et al., Design and characterization of a high-power induction module at megahertz repetition rate burst mode. Nucl. Instrum. Methods Phys. Res. Sect. A **579**(3), 941–950 (2007). doi:10.1016/j.nima.2007.06.016